Low-dissipation edge currents without edge states

Justin C. W. Song and Giovanni Vignale

Phys. Rev. B **99**, 235405 — Published 6 June 2019

DOI: 10.1103/PhysRevB.99.235405

Low-dissipation edge currents without edge states

Justin C. W. Song[1,2*] and Giovanni Vignale[3,4,5]
[1] *Division of Physics and Applied Physics, Nanyang Technological University, Singapore 637371*
[2] *Institute of High Performance Computing, Agency for Science, Technology, & Research, Singapore 138632*
[3] *Department of Physics and Astronomy, University of Missouri, Columbia, Missouri 65211, USA*
[4] *Center for Advanced 2D materials, National University of Singapore, Singapore 117542 and*
[5] *Yale-NUS College, 16 College Ave West, Singapore 138527*
(Dated: May 15, 2019)

We propose that bulk free carriers in topologically trivial multi-valley insulators with non-vanishing Berry curvature can give rise to low-dissipation edge currents, which are squeezed within a distance of the order of the valley diffusion length from the edge. This happens even in the absence of edge states [topological (gapless) or otherwise], and when the bulk equilibrium carrier concentration is thermally activated across the gap. Physically, the squeezed edge current arises from the spatially inhomogeneous valley orbital magnetization that develops from valley-density accumulation near the edge. While this current possesses neither topology nor symmetry protection and, as a result, is not immune to dissipation, in clean enough devices it can mimic low-loss ballistic transport.

I. INTRODUCTION

In bulk band insulators, carrier transport is exponentially activated, leading to a severely muted current response when an electric field is applied[1]. However, this adage fails spectacularly in topological matter where gapped bulk bands, characterized by a non-trivial topology[2,3], support gapless edge states[3–6], which can carry dissipationlesss charge currents along the edges of the sample. As a result, such edge currents have become synonymous with topologically non-trivial bulk bands as expected from the principle of bulk-edge correspondence[3,6–8].

Here we argue that in the presence of Bloch band Berry curvature, bulk free carriers in a multi-valley gapped insulator can conspire to produce a charge current that is squeezed close to sample boundaries *in the absence of edge states* (Fig. 1). The squeezed edge current (SEC) (Fig. 1**b**) has low (but finite) dissipation and occurs even when the equilibrium chemical potential is in the gap with a thermally activated bulk. As a result, SEC can act as a current conduit shunting the nominally insulating bulk to produce unusual non-activated resistivity characteristics at low temperature.

We expect SEC to naturally manifest in topologically trivial insulators possessing well-separated Bloch-band Berry curvature distributions[9] in the Brillouin zone (for e.g., in Fig. 1), such that the total integrated curvature is zero. As such, these systems do *not* possess gapless topologically protected edge states. Instead, the Berry curvature in each of the valleys enables valley Hall currents to be induced by an applied electric field and produce a valley density accumulation (of bulk carriers) near the edge of the sample, while the net charge density remains zero. The valley density gradient perpendicular to the edge produces a charge current flowing along the edge. This induced charge current (transverse to the valley density gradient) can be viewed as an anomalous transverse diffusion of carriers, with off-diagonal diffusion constants

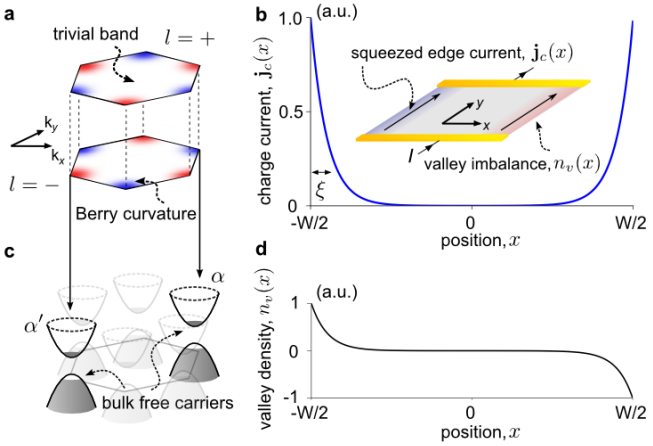

FIG. 1: **Squeezed edge currents in a topologically trivial insulator. a.** Berry curvature hot spots in topologically trivial insulator bands with zero net Berry flux over the entire Brillouin zone, e.g., (shown) Berry curvature, $\Omega_{l\alpha}$ hot spots for gapped graphene with broken inversion symmetry; $l=\pm$ are conduction and valence bands. **b.** A *charged* squeezed edge current (SEC), $\mathbf{j}_c(\mathbf{r})$, can flow along the sample edges [Eq. (9)] even in a gapped finite sized device (inset) without edge states. **c.** Carriers in highlighted bands at α,α' experience opposite signs of Berry curvature and contrasting transport characteristics (see text). **d.** Density imbalance between flavors/valleys can accumulate at sample edges over a width determined by the flavor/valley diffusion length, ξ, Eq. (7). We have used $\Omega_{l\alpha}$ for a gapped Dirac material (see text) so that $\sigma_H^v>0$ and $D_H^v<0$ [Eq. (4) and (5)].

of different signs in different valleys — a characteristic of carriers possessing finite Berry curvature.

SEC appears only in finite-sized samples (e.g., Hall-bar type geometries) and vanishes in the infinite bulk or when measurements exclude edge currents (e.g., Corbino geometries), see Fig. 2. While located close to sample boundaries, we emphasize that SEC arises from bulk carriers; it occurs in the absence of localized edge

modes of either topological (gapless) edge state origin or from other sources (e.g., band bending[10,11], gapped edge modes on rough boundaries[12]). Instead, SEC is intimately tied to a current-induced bulk and out-of-local-equilibrium magnetization build-up (pointing out-of-plane) at sample edges that has been recently measured in gapped Dirac systems[13,14]. The resulting out-of-local-equilibrium (magneto-electric) currents are the origin of the non-activated transport characteristics we unveil below.

While gapped graphene-type systems are not the only examples of this type of behavior, nevertheless, they present natural experimental targets due to their high quality, ease of manipulation, *lack* of topological gapless edge states, and clear observations of bulk valley Hall currents[15–17]. Indeed, a recent experiment that infers edge-type currents in topologically trivial systems[18] provide strong indications for SEC in gapped Dirac systems, see discussion below.

II. INHOMOGENEOUS VALLEY HALL CURRENTS

We begin by recalling that the position and velocity operators within a Bloch band (l) and valley (α) are

$$\hat{\mathbf{r}}_{l\alpha} = i\frac{\partial}{\partial \mathbf{k}} + \boldsymbol{\mathcal{A}}_{l\alpha}(\mathbf{k}), \quad \hat{\mathbf{v}}_{l\alpha} = \frac{1}{i\hbar}[\hat{\mathbf{r}}_{l\alpha}, \hat{H}]\,, \qquad (1)$$

where $\boldsymbol{\mathcal{A}}_{l\alpha}(\mathbf{k}) = i\langle u_{l\alpha}(\mathbf{k})|\nabla_{\mathbf{k}} u_{l\alpha}(\mathbf{k})\rangle$ is the Berry connection of the band and valley under consideration. We note that the band velocity reproduces the familiar $\langle u_{l\alpha}(\mathbf{k})|\hat{\mathbf{v}}_{l\alpha}|u_{l\alpha}(\mathbf{k})\rangle = \frac{d\epsilon_{l\alpha}(\mathbf{k})}{\hbar\partial\mathbf{k}} - \hbar^{-1}e\boldsymbol{\Omega}_{l\alpha}(\mathbf{k})\times\mathbf{E}$, where $\boldsymbol{\Omega}_{l\alpha}(\mathbf{k}) = \nabla_{\mathbf{k}}\times\boldsymbol{\mathcal{A}}_{l\alpha}(\mathbf{k})$ is the Berry curvature, $\epsilon_{l\alpha}$ is the band energy, and $-e<0$ is the electron charge. The Berry curvature is of order λ^2, where λ plays the role of an effective "Compton wavelength", inversely proportional to the gap at the band extrema (an explicit expression for "gapped graphene" will be given later). The above expressions are invariant under a gauge transformation that multiplies the Bloch wave function by a $\mathbf{k}$-dependent phase.

We now construct the current density fluctuation operator at wavevector $\mathbf{q}$ (for a single particle) as follows: $\hat{\mathbf{j}}_{l\alpha}(\mathbf{q}) = -\frac{e}{2}\left(\hat{\mathbf{v}}_{l\alpha}e^{-i\mathbf{q}\cdot\hat{\mathbf{r}}_{l\alpha}} + e^{-i\mathbf{q}\cdot\hat{\mathbf{r}}_{l\alpha}}\hat{\mathbf{v}}_{l\alpha}\right)$. We will be interested in current distributions that are slowly varying on the scale of λ. In this regime, we can expand $\hat{\mathbf{j}}_{l\alpha}(\mathbf{q})$ to first order in $\mathbf{q}$:

$$\hat{\mathbf{j}}_{l\alpha}(\mathbf{q}) = -e\hat{\mathbf{v}}_{l\alpha} + \frac{i}{2}e\left[(\mathbf{q}\cdot\hat{\mathbf{r}}_{l\alpha})\hat{\mathbf{v}}_{l\alpha} + \hat{\mathbf{v}}_{l\alpha}(\mathbf{q}\cdot\hat{\mathbf{r}}_{l\alpha})\right]. \qquad (2)$$

While the first term in Eq. (2) is the homogeneous current ($\mathbf{q}=0$) see Eq. (1), the second term only becomes relevant in an inhomogeneous system. Taking the latter's expectation value for state $|u_{l\alpha}(\mathbf{k})\rangle$ yields a purely transverse current $i\mathbf{q}\times\mathbf{m}_{l\alpha}(\mathbf{k})$, where $\mathbf{m}_{l\alpha}(\mathbf{k}) = -\frac{e}{4}\left(\hat{\mathbf{r}}\times\hat{\mathbf{v}} - \hat{\mathbf{v}}\times\hat{\mathbf{r}}\right)$ is the magnetic moment[19], see **Appendix**.

The full physical current density in real space $\mathbf{j}_{l\alpha}(\mathbf{r})$ proceeds directly from Eq. (2). Performing an inverse Fourier transformation, and averaging over a non-equilibrium state described by the inhomogeneous electron distribution function $f_{l\alpha}(\mathbf{k},\mathbf{r})$ yields

$$\begin{aligned}\mathbf{j}_{l\alpha}(\mathbf{r}) &= \sum_{\mathbf{k}}\left[-e\frac{\partial\epsilon_{l\alpha}(\mathbf{k})}{\hbar\partial\mathbf{k}} + \frac{e\boldsymbol{\Omega}_{l\alpha}(\mathbf{k})}{\hbar}\times e\mathbf{E}\right]f_{l\alpha}(\mathbf{k},\mathbf{r}) \\ &+ \sum_{\mathbf{k}}\frac{\partial f_{l\alpha}(\mathbf{k},\mathbf{r})}{\partial\mathbf{r}}\times\mathbf{m}_{l\alpha}(\mathbf{k})\,. \qquad (3)\end{aligned}$$

The first term of Eq. (3) is the familiar homogeneous current (including a homogeneous Hall current driven by an electric field)[20]. The second term is the current driven by an electron density gradient, and exists even in the absence of direct mechanical forces, such as an applied electric field[21,22]. As shown explicitly in **Appendix**, the latter is *Hall diffusion current* which must necessarily accompany electric field-driven Hall currents whenever the density is non-uniform.

We emphasize Eq. (3) is the full physical current that can be measured using local probes (e.g., via a scanning NV-center microscopy[23]). Even so, we note that in transport experiments, the charge current collected by leads attached to device boundaries are sensitive to the *net* charge current moving through the cross-section of the device. For example, charge transport is insensitive to circulating currents that may occur deep in the bulk, as illustrated in Ref.[24] by integrating through a device cross-section.

As a result, to ensure we capture the transport of charge we *explicitly take a cross-section over the entire sample* and integrate the net current flowing through it, see below. As we will see, these lead to SEC freely flowing in the same direction along the edges (Fig. 1), being fed by external contacts.

III. SQUEEZED EDGE CURRENTS

In order to illustrate SEC, we focus on a prototypical non-topological insulator: a gapped Dirac material where inversion symmetry is broken (e.g. gapped graphene on hexagonal Boron Nitride) with Hamiltonian around each of the valleys as: $\mathcal{H}_\alpha = v\hbar(k_x\tau_x + \alpha k_y\tau_y) + \Delta\tau_z$ (where $\tau_{x,y,z}$ are Pauli matrices) and $\alpha=\pm1$ for K,K' valleys respectively - see Fig. 1. The Berry curvature is concentrated in hot spots close to the two inequivalent valleys $\alpha=\{K,K'\}$ and is given by $\boldsymbol{\Omega}_{l\alpha}(\mathbf{k}) = -\frac{\alpha\lambda^2}{2}\frac{\Delta^3}{\epsilon_l^3(\mathbf{k})}\hat{\mathbf{z}}$, where $\lambda = \frac{\hbar v}{\Delta}$. The magnetic moment is given by $\mathbf{m}_{\ell\alpha}(\mathbf{k}) = \frac{e}{\hbar}\epsilon_{\mathbf{k},\ell}\boldsymbol{\Omega}_{\ell\alpha}(\mathbf{k})$ (see **Appendix**). For brevity, we will drop the vector notation for Berry curvature since $\boldsymbol{\Omega}(\mathbf{k}) = \Omega(\mathbf{k})\hat{\mathbf{z}}$ in two-dimensional systems. Total *charge current* (c) is determined by $\mathbf{j}_c \equiv \sum_{l,\alpha}\mathbf{j}_{l,\alpha}$ and the total *valley current* (v) is $\mathbf{j}_v \equiv \sum_{l\alpha}\alpha\mathbf{j}_{l,\alpha}$ where $\alpha=1$ for K and $\alpha=-1$ for K'. Similarly, we write charge and valley densities as $n_c \equiv \sum_{l,\alpha}n_{l\alpha}$ and $n_v \equiv \sum_{l,\alpha}\alpha n_{l\alpha}$; here

$n_{l\alpha}(\mathbf{r}) = \sum_{\mathbf{k}}(-e) f_{l\alpha}(\mathbf{k},\mathbf{r})$ is the charge density in l,α.

Since $\Omega_{l\alpha}(\mathbf{k})$ changes sign in going from $\alpha = K$ to $\alpha = K'$, the flow of charge currents is particularly sensitive to the imbalance of distribution function between valleys. To see this, using Eq. (3), we construct the total charge and valley currents in each band l explicitly as

$$\begin{aligned} \mathbf{j}_c &= -D\boldsymbol{\nabla} n_c + \sigma\mathbf{E} - D_H^v[(\boldsymbol{\nabla} n_v)\times\hat{\mathbf{z}}], \\ \mathbf{j}_v &= -D\boldsymbol{\nabla} n_v + [\sigma_H^v]\hat{\mathbf{z}}\times\mathbf{E} - D_H^v[(\boldsymbol{\nabla} n_c)\times\hat{\mathbf{z}}], \end{aligned} \quad (4)$$

where D is the ordinary *longitudinal* diffusion constant of carriers within the bands, σ is the longitudinal conductivity, and $[\sigma_H^v] = (e^2/\hbar)\sum_{\mathbf{k},l,\alpha}\alpha\Omega_{l\alpha} f_{l\alpha}^{(0)}(\mathbf{k})$ is the valley Hall conductivity, with $f_{l\alpha}^{(0)}(\mathbf{k})$ is the Fermi-Dirac function $f_{l\alpha}^{(0)}(\mathbf{k}) = \{1+\exp\big[(\epsilon_l(\mathbf{k})-\mu_{l\alpha})/(k_BT)\big]\}^{-1}$ with $\mu_{l\alpha}$ the (quasi-) chemical potential. Crucially, D_H^v is the *valley Hall diffusion constant*, which captures the transverse current flow arising from an inhomogeneous distribution function in each of the valleys: $\mathbf{j}_{l\alpha} = -D_H^{l\alpha}\boldsymbol{\nabla} n_{l\alpha}\times\hat{\mathbf{z}}$, where for gapped graphene we have

$$D_H^{l\alpha} = \frac{\sum_{\mathbf{k}}\epsilon_l(\mathbf{k})\Omega_{l\alpha}(\mathbf{k})\frac{\partial f_{l\alpha}^{(0)}(\mathbf{k})}{\partial\mu_{l\alpha}}}{\hbar\sum_{\mathbf{k}}\frac{\partial f_{l\alpha}^{(0)}(\mathbf{k})}{\partial\mu_{l\alpha}}}. \quad (5)$$

Since $\Omega_{l\alpha}(\mathbf{k})$ changes sign when either the band index or the valley index is switched, $D^{+,\alpha} = D_H^{-,\alpha} = \alpha D_H^v$, where $D_H^v \equiv D_H^{l=+,\alpha=+1}$. Summing $\mathbf{j}_{l\alpha}$ over l and α gives the inhomogeneous charge current as written in Eq. (4).

When an electric field is applied along the sample, the bulk valley Hall effect produces a valley Hall current which must be cancelled by a valley density gradient perpendicular to the sample boundaries. This dramatically impacts *charge* transport characteristics. The profiles of density imbalance between valleys in each band $n_v(\mathbf{r})$ obey the diffusion equation

$$\partial_t n_v(\mathbf{r}) - D\nabla^2 n_v(\mathbf{r}) + \frac{n_v(\mathbf{r})}{\tau_v} = -\boldsymbol{\nabla}\cdot([\sigma_H^v]\hat{\mathbf{z}}\times\mathbf{E}), \quad (6)$$

where τ_v is the intervalley scattering time between valleys which captures the rate at which disparate parts (at K and K') of the Fermi surface equilibrate with each other. In the non-degenerate limit, the longitudinal diffusion can be estimated as $D = k_BT\eta/e$ where η is the mobility; here we have used the same diffusion constant in both conduction and valence bands for simplicity. Different diffusion constants can be implemented with no qualitative change to the results below.

Considering a long Hall bar, $L \gg W$, we treat $n_v(\mathbf{r})$ and $\mathbf{E}(\mathbf{r})$ as independent of y along the bar; this reduces Eq. (6), in the steady state, to a one-dimensional differential equation, with the density jumping from a finite value to zero at $x = \pm W/2$. Further, by focusing on regions far away from contacts, we treat the electric field as uniform. As a result, $n_v(\mathbf{r})$ is driven only by delta-function sources at the boundaries $x = \pm W/2$: $-\boldsymbol{\nabla}\cdot([\sigma_H^v]\hat{\mathbf{z}}\times\mathbf{E}) = -[\sigma_H^v]E\,[\delta(x-W/2)-\delta(x+W/2)]$, where $\mathbf{E} = E\hat{\mathbf{y}}$. We note that σ_H^v is maximal when the chemical potential is in the gap[25].

The solution of the differential equation is found by elementary means to be

$$n_v(x) = -\frac{[\sigma_H^v]E\tau_v}{\xi\cosh(W/2\xi)}\sinh\left(\frac{x}{\xi}\right), \quad (7)$$

for $|x| \le W/2$ and 0 otherwise. Here $\xi = \sqrt{D\tau_v}$ is the valley diffusion length. As shown in Fig. 1**d**, valley density accumulates at the edges.

We emphasize that our diffusive treatment is valid only when the spatial profile of $n_v, \mathbf{j}_c$ is slowly varying on the scale of the Compton wavelength $\lambda = \hbar v/\Delta$, the typical length scale of the wavepackets close to the band edge in a gapped Dirac model. $\lambda \simeq 6\times10^{-8}$ m for $v = 10^6\,\mathrm{m\,s^{-1}}$ and half-gap size $\Delta = 10\,\mathrm{meV}$. The typical scale of $n_v(\mathbf{r})$ variation is captured by the diffusion length ξ. As a result, we expect that our semi-classical diffusive picture holds as long as $\xi \gg \lambda$. Using the non-degenerate form of longitudinal diffusion constant $D = k_BT\eta/e$ we find this occurs for large enough temperatures

$$T \gg T_0, \quad k_BT_0 = \frac{e\lambda^2}{\eta\tau_v}. \quad (8)$$

Using a mobility $\eta = 1\,\mathrm{m^2/(Vs)}$, $\tau_v = 10\,\mathrm{ps}$ we estimate $k_BT_0 \approx 0.4\,\mathrm{meV}$ ($T_0 \approx 5\,\mathrm{K}$). Below this temperature scale (set by T_0), a fully quantum mechanical treatment is needed which is beyond the scope of the present work. In spite of this, the temperature regime $\Delta > T > T_0$ (in which our treatment is valid) defines a large and technologically important temperature regime.

Applying the inhomogeneous valley density profile in Eq. (7) to Eq. (4) yields a charge current density flowing along the edge (see Fig. 1) as

$$\mathbf{j}_c^{\mathrm{SEC}}(\mathbf{r}) = j_c^{\mathrm{SEC}}(\mathbf{r})\hat{\mathbf{y}}, \quad j_c^{\mathrm{SEC}}(\mathbf{r}) = D_H^v\partial_x n_v(\mathbf{r}). \quad (9)$$

In the limit $\xi \ll W$, $\mathbf{j}_c^{\mathrm{SEC}}(\mathbf{r})$ form squeezed quasi-one-dimensional channels flowing along the edges of the Hall bar. Crucially, Eq. (9) yields two squeezed current channels flowing in the *same* direction as shown in Fig. 1; $\mathbf{j}_c^{\mathrm{SEC}}(\mathbf{r})$ flows along $\mathbf{E}$. This demonstrates that the diffusion current arising from the inhomogeneous electron distribution [see Eq. (3)] is *not* circulating, but contributes to total charge transport in the device.

Integrating the current density over one of these SEC channels and writing $E = V/L$ where V is the voltage drop over length L yields $I_{\mathrm{SEC}} = \int_0^{W/2} j_c^{\mathrm{SEC}}(x)dx = -D_H^v\sigma_H^v\tau_v V/(\xi L)$. I_{SEC} constitutes a distinctly new parallel channel for current to flow in the Hall bar. We note that $-D_H^v\sigma_H^v$ is positive, see Fig. 1. Adding the current flowing in the bulk, as well as accounting for contact resistance, we find the device resistance

$$R^{-1} = R_{\mathrm{bulk}}^{-1} + R_{\mathrm{SEC}}^{-1},\ R_{\mathrm{SEC}} = (\rho_{1\mathrm{d}}L) + R_{\mathrm{contact}}, \quad (10)$$

where $\rho_{1\mathrm{d}} = \xi/(|D_H^v\sigma_H^v|\tau_v)$, and R_{bulk} is the resistance of the bulk. Crucially, D_H^v, σ_H^v arise from the Berry curvature of the bands and exhibit a non-activated behavior

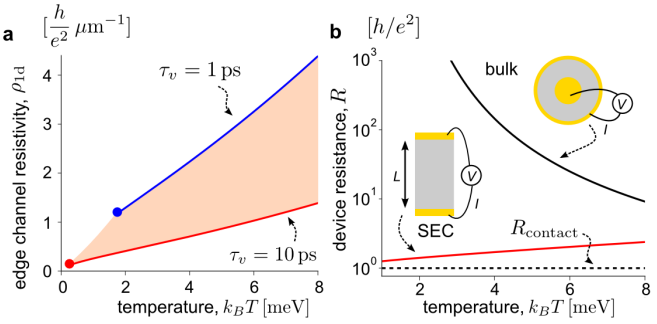

FIG. 2: **Low dissipation squeezed edge channels. a**. One-dimensional resistivity of a single squeezed edge current (SEC) channel along the edge of gapped graphene device [Eq. (12)] shown for $\tau_v = 10\,\mathrm{ps}$ (red dashed) and $\tau_v = 1\,\mathrm{ps}$ (blue dashed). τ_v in-between these two values occupy the shaded orange region. Red and blue dots indicate temperature T_0 above which the semi-classical treatment is valid for the respective τ_v [see Eq. (8)]. **b**. Device resistance for a Hall-bar device (red, $L = 1\,\mu\mathrm{m}$ and $\tau_v = 10\,\mathrm{ps}$) and a Corbino device (black). For illustration we used parameters: $\Delta = 15\,\mathrm{meV}$, $\eta = 2\,\mathrm{m}^2/\mathrm{Vs}$, and $\sigma_H^v = 2e^2/h$. Here we have taken a value of $R_{\mathrm{contact}} = h/e^2$ for illustration; other R_{contact} values can be used with no qualitative changes.

in temperature, even when the chemical potential is in the gap. As we will see, this yields ρ_{1d} that does not exponentially rise at low temperatures in stark contrast with R_{bulk} that exponentially rises at low temperatures.

IV. LOW DISSIPATION SEC CHANNELS

In the non-degenerate limit $\mu_{l\alpha}, k_BT \ll \Delta$, we estimate $\sigma_H^v \approx 2e^2/h$ for an almost fully filled band (accounting for spin degeneracy). Similarly, D_H^v can be estimated from Eq. (5) in the same limit as

$$D_H^{l\alpha} \approx \alpha \frac{\hbar v^2}{2\Delta}\mathcal{F}(\tilde{\beta}), \quad \mathcal{F}(\tilde{\beta}) = \Big[\frac{-\tilde{\beta}^2 \mathrm{Ei}(-\tilde{\beta})}{(1+\tilde{\beta})\exp(-\tilde{\beta})}\Big], \quad (11)$$

where $\tilde{\beta} = \Delta/k_BT$, $\mathrm{Ei}(x) = -\int_{-x}^{\infty} dt e^{-t}/t$ is the exponential integral, and we have approximated $(1 + \exp[\tilde{\beta}])^{-1} \approx \exp[-\tilde{\beta}]$ for $\tilde{\beta} \gg 1$. Interestingly for small T, $\mathcal{F} \to 1$, reflecting the (band) geometrical origin of anomalous transverse diffusion. We note that σ_H^v, D_H^v do not vary significantly for **E**-induced shifts in $\mu_{l\alpha} < \Delta$; sizeable valley imbalances along the edge can accumulate in the linear response regime.

Writing $D_H^v = D_H^{l,(\alpha=+1)}$ [see Eq. (5)] yields the resistivity of the quasi-1D channels along the sample edges

$$\rho_{1d}(T) = \frac{\rho_0}{\tilde{\beta}^{1/2}\mathcal{F}(\tilde{\beta})}, \quad \rho_0 = \frac{2\Delta^{3/2}(\eta/e)^{1/2}}{\hbar v^2 \tau_v^{1/2}|\sigma_H^v|} \quad (12)$$

where ρ_0 is the characteristic 1D resistivity, see also **Appendix**.

ρ_0 is non-universal and depends on the rate of relaxation of different parts of the Fermi surface at K and K' encoded in the intervalley scattering time τ_v. In a bulk homogeneous sample with few short-range impurities, intervalley scattering can be long (on the order of ten to several tens of picoseconds[15–17]). Further, it has been noticed in Ref. [26] that the notion of valleys is preserved for *generic* edge terminations in graphene since generic terminations are described by zig-zag-type boundary conditions. Even so, the specific edge termination configuration may enable enhanced intervalley scattering (as compared with the bulk), for example through edge roughness or via indirect scattering processes through flat/weakly-dispersive edge states[27], and the value of τ_v can be accordingly reduced close to edges. For these reasons, in Fig. 2 we have chosen to illustrate SEC by presenting the values of $\rho_{1d}(T)$ associated with a range of values of $\tau_v \sim 1 - 10\,\mathrm{ps}$. Strikingly, even for relatively fast inter-valley scattering $\tau_v \sim 1\,\mathrm{ps}$, ρ_{1d} can still take on small values $\rho_{1d} \sim h/e^2\mu\mathrm{m}^{-1}$, see Fig. 2**a** (red curve). In contrast, the bulk resistance exponentially rises at low temperatures, $R_{\mathrm{bulk}} \propto \exp(\Delta/k_BT)$, where Δ is the half-gap size. As a result, for small gap sizes of tens of meV, sufficiently short lengths, and low temperatures, SEC possess a very small resistivity [dominating R^{-1} in Eq. (10)], and can mimic low-dissipation quasi-one-dimensional channel that shunts the bulk, see Fig. 2**b**.

We note that in the low-temperature regime where $(\rho_{1d}L) \ll R_{\mathrm{contact}}$, Eq. (10) is dominated by the contact resistance, see Fig. 2b. As a result of the low-dissipation in the SEC channel, current-voltage characteristics in a two-terminal geometry may display only very weakly L-dependent characteristics.

V. DISCUSSION

It is useful to point out some of the conceptual differences between conventional bulk transport in electronic systems and SEC. Bulk carrier transport in electronic systems is typically characterized by a *homogeneous flow* of current density through the sample that is sustained by an electric field that accelerates the charge carriers. This electric field displaces the Fermi surface in momentum space so that larger current density corresponds to a larger relative displacement of the Fermi surface in momentum space. In contrast, SEC arises from an *inhomogeneous flow* of current density running along the edges of the device. For SEC, the charge carriers are not accelerated along the flow direction (**y**), instead SEC is sustained by an inhomogeneous valley density profile $n_v(x)$ in real space (along **x**) induced by an electric field (along **y**).

Crucially, larger SEC current corresponds to a larger local steady-state valley density (close to the edges in real space), see Eq. (9). Interestingly, as detailed below, *even in the linear response regime*, this *steady-state*

out-of-equilibrium valley density can be far larger than equilibrium density of thermally activated carriers when the chemical potential is in the gap and at low temperatures. This is in stark contrast to what is expected in conventional bulk transport, where electronic density is kept uniform and close to its equilibrium value even when current is flowing through. Where does this large density of carriers come from? As we now argue, the increased local steady-state valley density can be fed by the source/drain contacts which inject carriers that are shunted along the SEC channels. This can be understood as follows. Charge transport occurs when carriers are injected from a source contact, and removed at a drain contact. After short time transients, the device reaches a steady-state with the amount of current injected (at source contact) equal to the amount of current removed (at drain contact) resulting in a steady state distribution of carriers. For our system, this steady-state out-of-equilibrium distribution of carriers is determined by Eq. (6) allowing sizeable steady-state local valley densities to be accumulated along the edges.

We now estimate the maximal valley density, n_v^*, that can be accumulated along the edges [as determined by Eq. (6)] concentrating on the regime of μ in the gap and $k_BT < \Delta$. To proceed, we note that the validity of linear response theory requires that the values of D, σ_{xy}^v (as well as D_H^v when considering the SEC current, see below) used do not change much as valley density is accumulated at the edge of the sample. For gapped graphene with equilibrium chemical potential initially in the gap, this requires the electric-field induced change in the quasi-Fermi levels (close to the edges) to satisfy $\delta\mu_{e,h}^{K,K'} \ll \Delta$. This is because the relevant transport coefficients for SEC (D, σ_{xy}^v and D_H^v) do not vary appreciably as chemical potential is changed inside the gap[28]; in fact, σ_{xy}^v and D_H^v both reach their maximal values inside the gap. The condition on quasi-Fermi levels can be immediately translated into one for density so that linear response is satisfied for $n_v \ll n_v^*$ where $n_v^* = \mathcal{N}\int_\Delta^\infty d\epsilon \nu(\epsilon)\big[1+\exp[(\epsilon-\Delta)/k_BT]\big]^{-1}$, where $\nu(\epsilon)$ is the density of states, and $\mathcal{N}$ is the valley/flavor and spin degeneracy. Using the density of states of a gapped Dirac cone, we obtain

$$n_v^* = \mathcal{N}\big[12\ln(2)k_BT\Delta + \pi^2(k_BT)^2\big]/(24\pi v^2\hbar^2). \quad (13)$$

Unusually, $n_v^* \propto T$ can be much larger than the thermally activated carrier density at equilibrium [$n_T^{\rm eq} \propto \exp(-\Delta/k_BT)$]. As discussed above, this *steady-state* n_v builds up and is fed by the source/drain contacts that inject/remove a steady flow of carriers.

A related quantity is the critical SEC, I^*, that can be be carried by the system through the SEC channels along the edges ($I_{\rm SEC} \ll I^*$) in order to remain in the linear response regime. Since $\mathbf{j}_c^{\rm SEC}$ is directly proportional to the amplitude of $n_v(x)$, see Eq. (9), and integrating over the SEC channel width we obtain the critical SEC current as

$$I^* = eD_H^v n_v^* \approx \frac{e\mathcal{N}}{2h}k_BT\ln 2 + \mathcal{O}(T^2/\Delta), \quad (14)$$

where in the last line we have used the value of D_H^v in Eq. (11) for small T, substituted Eq. (13), and kept the leading terms in T. Taking $\mathcal{N} = 4$ and taking $k_BT = 1\,$meV we obtain sizeable $I^* \sim 0.053\,\mu$A, allowing significant SEC to be run through the device with low dissipation. Interestingly, we note that I^* vanishes as $T \to 0$ indicating that while SEC resistivity slowly decreases as T decreases, the amount of current these channels can sustain (in the linear response regime) also vanishes.

The non-activated conductance as well as non-activated valley density sustained at the edges of the sample of SEC is distinct from that of conventional transport. Indeed, the fact that valley densities n_v^* that can be sustained are far larger than the thermally activated density at equilibrium $n_T^{\rm eq}$ suggests that SEC is an out-of-*local*-equilibrium effect; nevertheless it can still possess linear response characteristics, as detailed above.

SEC here replicates the unusual transport characteristics found in recent gapped graphene-type structures (G/hBN and gapped Bilayer graphene devices)[18]. For example, Fig. 1 mirrors the sharp spatial edge current distribution in gapped graphene-type structures found in Ref.[18] using Josephson current spectroscopy. Further, a saturation of device resistance (up to a few resistance quanta) was measured in Hall bars even at low temperatures ($\sim 10\,$K) while Corbino geometry measurements of the same samples showed fully activated behavior; this directly reproduces SEC characteristics in Fig. 2b. Further, we note recent Kerr-rotation microscopy in biased monolayer MoS_2 show magnetization accumulated along edges[13,14], another signature of valley imbalance accumulation and SEC along the edge. We emphasize that while neither gapped graphene (G/hBN or gapped bilayer graphene) nor MoS_2 possess topological gapless edge states, they possess strong Berry curvature close to their band edges, enabling the unusual quantum geometry mediated transport (such as SEC) in these systems[13,14,18].

Bloch band quantum geometry can play a crucial role in charge transport of time-reversal invariant materials as epitomized by SEC that mimic ballistic edge channels without (spectral) edge states. SEC exhibits striking non-activated behavior even in nominally bulk insulating and topologically trivial devices. Additionally, SEC also mediates spin-free magneto-electric coupling, an unusual characteristic of these "trivial" insulators with non-vanishing Berry curvature; band geometry naturally interlaces charge and magnetization degrees of freedom even in a spin-orbit free system.

Acknowledgements - We gratefully acknowledge useful conversations with Dima Pesin, Mark Runder, Maksym Serbyn, and Valla Fatemi. J.C.W.S. acknowledges support from the Singapore National Research

Foundation (NRF) under NRF fellowship award NRF-NRFF2016-05 as well as the Nanyang Technological University Singapore through a start-up grant. G.V. acknowledges generous support from the CA2DM, where this work was initiated, and from NSF Grant DMR-1406568.

* Electronic address: justinsong@ntu.edu.sg

[1] N. W. Ashcroft, and N.D. Mermin, *Solid State Physics*, Brooks/Cole Cengage Learning, California, (1976).

[2] D. J. Thouless, M. Kohmoto, M. P. Nightingale, and M. den Nijs, "Quantized Hall conductance in a two-dimensional periodic potential " Physical Review Letters **49** 405 (1982)

[3] X. G. Wen, *Quantum field theory of many-body systems: from the origin of sound to an origin of light and electrons.* Oxford University Press (2004).

[4] B. I. Halperin, "Quantized Hall conductance, current-carrying edge states, and the existence of extended states in a two-dimensional disordered potential" Physical Review B **25** 2185 (1982).

[5] M. Büttiker, "Absence of backscattering in the quantum Hall effect in multiprobe conductors" Physical Review B **38** 9357 (1988)

[6] M. Z. Hasan, and C. L. Kane. "Colloquium: topological insulators " Reviews of Modern Physics 82.4 (2010): 3045.

[7] Y. Hatsugai, "Chern number and edge states in the integer quantum Hall effect " Physical Review Letters **71** 3697 (1993).

[8] A. H. Macdonald, P Streda, "Quantized Hall effect and edge currents", Physical Review B **29**, 1616 (1984).

[9] D. Xiao, W. Yao, and Q. Niu, "Valley-contrasting physics in graphene: magnetic moment and topological transport." Physical Review Letters **99** 236809 (2007)

[10] N. Fabrizio, H. J. Suominen, M. Kjaergaard, C. M. Marcus, E. Sajadi, J. A. Folk, F. Qu, A. J. A. Beukman, F. K. de Vries, J. van Veen, S. Nadj-Perge, L. P. Kouwenhoven, B.-M. Nguyen, A. A. Kiselev, W. Yi, M. Sokolich, M. J. Manfra, E. M. Spanton, K. A. Moler, "Edge transport in the trivial phase of InAs/GaSb" New Journal of Physics **18** 083005 (2016).

[11] A. J. A. Beukman, "Topology in two-dimensional systems" section 7.3, PhD Thesis TU Delft (2016).

[12] J. Li, I. Martin, M. Büttiker, A. F. Morpurgo, "Topological origin of subgap conductance in insulating bilayer graphene." Nature Physics 7.1 (2011): 38.

[13] J. Lee, K.F. Mak, and J. Shan. "Electrical control of the valley Hall effect in bilayer MoS 2 transistors." Nature nanotechnology **11** 421 (2016).

[14] J. Lee, Z. Wang, H. Xie, K. F. Mak, and J. Shan, "Valley magnetoelectricity in single-layer MoS_2"' Nature materials, **16** 887 (2017).

[15] R. V. Gorbachev, J. C. W. Song, G. L. Yu, A. V. Kretinin, F. Withers, Y. Cao, A. Mishchenko, I. V. Grigorieva, K. S. Novoselov, L. S. Levitov, A. K. Geim, "Detecting topological currents in graphene superlattices" Science **346** 448-451 (2014)

[16] Y. Shimazaki, M. Yamamoto, I. V. Borzenets, K. Watanabe, T. Taniguchi, S. Tarucha, "Generation and detection of pure valley current by electrically induced Berry curvature in bilayer graphene" Nature Physics **11** 1032-1036 (2015)

[17] M. Sui, G. Chen, L. Ma, W. Shan, D. Tian, K. Watanabe, T. Taniguchi, X. Jin, W. Yao, D. Xiao, Y. Zhang, "Gate-tunable topological valley transport in bilayer graphene", Nature Physics **11** 1027-1031 (2015).

[18] M. J. Zhu, A. V. Kretinin, M. D. Thompson, D. A. Bandurin, S. Hu, G. L. Yu, J. Birkbeck, A. Mishchenko, I. J. Vera-Marun, K. Watanabe, T. Taniguchi, M. Polini, J. R. Prance, K. S. Novoselov, A. K. Geim, M. Ben Shalom, "Edge currents shunt the insulating bulk in gapped graphene", Nature Communications **8** 14552 (2017).

[19] J. Shi, G. Vignale, D. Xiao, and Q. Niu, "Quantum theory of orbital magnetization and its generalization to interacting systems", Physical Review Letters **99**, 197202 (2007).

[20] Xiao, Di, Ming-Che Chang, and Qian Niu, "Berry phase effects on electronic properties", Reviews of modern physics **82** 1959 (2010)

[21] D. Xiao., Y. Yao, Z. Fang, and Q. Niu ,"Berry-phase effect in anomalous thermoelectric transport", Physical Review Letters, **97** 026603 (2006).

[22] D. T. Son, and N. Yamamoto, "Berry curvature, triangle anomalies, and the chiral magnetic effect in Fermi liquids" Physical Review Letters **109** 181602 (2012).

[23] J. P. Tetienne, N. Dontschuk, D. A. Broadway, A. Stacey, D. A. Simpson, L. C. Hollenberg, "Quantum imaging of current flow in graphene" Science Advances, **3**, e1602429 (2017).

[24] N. R. Cooper, B. I Halperin, and I. M. Ruzin, "Thermoelectric response of an interacting two-dimensional electron gas in a quantizing magnetic field", Physical Review B **55**, 2344 (1997).

[25] Y. D. Lensky, J. C. W. Song, P. Samutpraphoot, L. S. Levitov, "Topological valley currents in gapped Dirac materials" Physical Review Letters **114** 25 (2015).

[26] A. R. Akhmerov, and C. W. J. Beenakker. "Boundary conditions for Dirac fermions on a terminated honeycomb lattice." Physical Review B 77.8 (2008): 085423.

[27] L. Jian, A. F. Morpurgo, M. Büttiker, and I. Martin, "Marginality of bulk-edge correspondence for single-valley Hamiltonians." Physical Review B **82** 245404 (2010).

[28] This behavior is in juxtaposition to that expected of the bulk longitudinal conductivity, which is exponentially sensitive to small changes in (quasi-) chemical potential in the gap.

Appendix A: Covariant derivative and anomalous velocity

As a warm-up, we briefly review the covariant derivative. Our starting point is the gauge invariant (physical) position operator in the Bloch representation

$$\hat{\mathbf{r}}_{l\alpha} = i\frac{\partial}{\partial \mathbf{k}} + \boldsymbol{\mathcal{A}}_{l\alpha}(\mathbf{k}) \tag{A1}$$

where $\boldsymbol{\mathcal{A}}_{l\alpha}(\mathbf{k}) = i\langle u_{l\alpha}(\mathbf{k})|\partial_{\mathbf{k}} u_{l\alpha}(\mathbf{k})\rangle$ is the Berry connection of the band and valley under consideration. We note

that $i\frac{\partial}{\partial \mathbf{k}}$ is the canonical (non-gauge-invariant) position operator in the momentum representation. Crucially, different components of $\hat{\mathbf{r}}$ do not commute with each other. In particular,

$$[\hat{r}_i, \hat{r}_j] = i\Big(\partial_{k_i}[\mathcal{A}_{l\alpha}]_j - \partial_{k_j}[\mathcal{A}_{l\alpha}]_i\Big) \equiv i\varepsilon_{ijk}\Omega_k \tag{A2}$$

where the Berry curvature is

$$\Omega_i \equiv \varepsilon_{ijk}\partial_{k_j}[\mathcal{A}_{l\alpha}]_k\,. \tag{A3}$$

In the presence of an applied electric field, the Hamiltonian reads as $\hat{H} = \epsilon_n(\mathbf{k}) - (-e)\mathbf{E}\cdot\hat{\mathbf{r}}$. Here $-e<0$ is the electron charge, and $\mathbf{E}$ is the electric field. Writing the velocity as $\hat{\mathbf{v}} = \frac{1}{i\hbar}[\hat{\mathbf{r}}, \hat{H}]$, we obtain

$$\langle \hat{v}_i\rangle = \frac{1}{i\hbar}\langle [r_i, \hat{H}]\rangle = \frac{1}{\hbar}\frac{\partial \epsilon_n(\mathbf{k})}{\partial_{k_i}} - \frac{ie}{\hbar}\langle [\hat{r}_i, \hat{r}_j]\rangle E_j \tag{A4}$$

$$= \frac{1}{\hbar}\frac{\partial \epsilon_n(\mathbf{k})}{\partial_{k_i}} + \frac{e}{\hbar}\varepsilon_{ijk}E_j\Omega_k, \tag{A5}$$

where the second term is the anomalous velocity.

Appendix B: Magnetic moment and inhomogeneous current density

In this section, we discuss the relationship between the magnetic moment and the inhomogeneous current density in Eq. (2) of the main text.

We begin by noting that the magnetic moment,

$$\begin{aligned}\hat{\mathbf{m}} &= -\frac{e}{4}\left(\hat{\mathbf{r}}\times\hat{\mathbf{v}} - \hat{\mathbf{v}}\times\hat{\mathbf{r}}\right)\\ &= \frac{ie}{4\hbar}\left(\hat{\mathbf{r}}\times[\hat{\mathbf{r}}, \hat{H}] - [\hat{\mathbf{r}}, \hat{H}]\times\hat{\mathbf{r}}\right),\end{aligned} \tag{B1}$$

where $\hat{H}$ is the hamiltonian and $\hat{\mathbf{v}} = -i\hbar^{-1}[\hat{\mathbf{r}}, \hat{H}]$. It is important to notice that at this stage the operator $\hat{\mathbf{r}}$ is not yet projected on a given band. Thus, interband matrix elements of $\hat{\mathbf{r}}$ are still included. However the hamiltonian is diagonal in the band representation. The magnetic moment can be re-expressed in component form as

$$m_i = \frac{ie}{4\hbar}\varepsilon_{ijk}\left(\hat{r}_j\hat{r}_k\hat{H} - \hat{r}_j\hat{H}\hat{r}_k - \hat{r}_j\hat{H}\hat{r}_k + \hat{H}\hat{r}_j\hat{r}_k\right), \tag{B2}$$

where a sum over repeated indices is implied. This can be recast as

$$\begin{aligned}&i\varepsilon_{ijk}q_jm_k\\ &= \frac{e}{2\hbar}q_j\left[\hat{r}_i\hat{H}\hat{r}_j - \hat{r}_j\hat{H}\hat{r}_i\right]\\ &- \frac{e}{2\hbar}q_j\left[\frac{\hat{H}(\hat{r}_i\hat{r}_j - \hat{r}_j\hat{r}_i)}{2} + \frac{(\hat{r}_i\hat{r}_j - \hat{r}_j\hat{r}_i)\hat{H}}{2}\right].\end{aligned} \tag{B3}$$

Now we make use of the commutation relation

$$\hat{\mathbf{r}}\times\hat{\mathbf{r}} = i\hat{\mathbf{\Omega}}\,, \tag{B4}$$

where $\hat{\mathbf{\Omega}}$ is the Berry curvature *operator* defined as the covariant derivative of the Berry connection in the full Hilbert space, to rewrite m_i as

$$m_i = -\frac{ie}{2\hbar}\varepsilon_{ijk}\hat{r}_j\hat{H}\hat{r}_k - \frac{e}{4\hbar}\left[\hat{\Omega}_i\hat{H} + \hat{H}\hat{\Omega}_i\right]. \tag{B5}$$

We can now take the diagonal matrix element of this operator in the band of interest, say $l\alpha$, and noting that $\hat{\mathbf{r}} = i\boldsymbol{\nabla}_{\mathbf{k}}$, where $\boldsymbol{\nabla}_{\mathbf{k}} = \partial_{\mathbf{k}} - i\boldsymbol{\mathcal{A}}(\mathbf{k})$ is the covariant derivative (still an operator in the full Hilbert space), and that the diagonal matrix element of $\hat{\mathbf{\Omega}}$ is

$$\Omega_{l\alpha}(\mathbf{k}) = i\langle\nabla_{\mathbf{k}}u_{l\alpha}(\mathbf{k})|\times|\nabla_{\mathbf{k}}u_{l\alpha}(\mathbf{k})\rangle\,, \tag{B6}$$

we recover the well-known formula[19,20]

$$\mathbf{m}_{l\alpha}(\mathbf{k}) = \frac{ie}{2\hbar}\langle\nabla_{\mathbf{k}}u_{l\alpha}(\mathbf{k})|(\epsilon_{l\alpha}(\mathbf{k}) - \hat{H})\times|\nabla_{\mathbf{k}}u_{l\alpha}(\mathbf{k})\rangle\,. \tag{B7}$$

Similarly, we write the q-linear part of the current density operator in Eq. (2) of the main text (denoted by $\hat{\mathbf{j}}^{(1)}_{\mathbf{q},i}$) in component form as

$$\begin{aligned}\hat{j}^{(1)}_{\mathbf{q},i} &= i\frac{e}{2}q_i\left(\hat{v}_j\hat{r}_i + \hat{r}_i\hat{v}_j\right)\\ &= \frac{e}{2\hbar}q_i\left(\hat{r}_j\hat{H}\hat{r}_i - \hat{H}\hat{r}_j\hat{r}_i + \hat{r}_i\hat{r}_j\hat{H} - \hat{r}_i\hat{H}\hat{r}_j\right)\end{aligned} \tag{B8}$$

After some algebra, this can be recast in the following form:

$$\begin{aligned}\hat{j}^{(1)}_{\mathbf{q},i} &= \frac{e}{2\hbar}q_j\left[\hat{r}_i\hat{H}\hat{r}_j - \hat{r}_j\hat{H}\hat{r}_i\right]\\ &- \frac{e}{2\hbar}q_j\left[\frac{\hat{H}\,(\hat{r}_i\hat{r}_j - \hat{r}_j\hat{r}_i)}{2} + \frac{(\hat{r}_i\hat{r}_j - \hat{r}_j\hat{r}_i)\,\hat{H}}{2}\right]\\ &+ \frac{e}{2\hbar}q_i\left[\hat{H}\frac{\hat{r}_i\hat{r}_j + \hat{r}_j\hat{r}_i}{2} - \frac{\hat{r}_i\hat{r}_j + \hat{r}_j\hat{r}_i}{2}\hat{H}\right]\end{aligned} \tag{B9}$$

The first two lines of this equation reproduce Eq. (B3) exactly. The last line is, in general, nonzero, but vanishes when averaged in a single band because the $\hat{H}$ operators become numbers $\hat{H}\to\epsilon_{l\alpha}(\mathbf{k})$ and what remains is the difference of two identical terms. We conclude that

$$[\hat{j}^{(1)}_{\mathbf{q},i}]_{l\alpha} = i\varepsilon_{ijk}q_jm_{l\alpha,k} \tag{B10}$$

or, in real space,

$$[\hat{\mathbf{j}}^{(1)}(\mathbf{r})]_{l\alpha} = \boldsymbol{\nabla}_{\mathbf{r}}\times\mathbf{m}_{l\alpha}(\mathbf{r})\,. \tag{B11}$$

Taking $\mathbf{m}_{l\alpha}(\mathbf{r}) = \sum_{\mathbf{k}} f_{l\alpha}(\mathbf{k},\mathbf{r})\mathbf{m}_{l\alpha}(\mathbf{k})$ we recover Eq. (3) of the main text.

Appendix C: Magnetic moment for gapped graphene

Here we briefly derive (for the convenience of the reader) the well-known relation between Berry curvature and the magnetic moment for gapped graphene, namely:

$$\mathbf{m}_{\ell\alpha}(\mathbf{k}) = \frac{e}{\hbar}\epsilon_{\mathbf{k},\ell}\mathbf{\Omega}_{\ell\alpha}(\mathbf{k}). \tag{C1}$$

Eq. (C1) can be shown in a straightforward fashion by recalling that magnetic moment is

$$\langle\hat{\mathbf{M}}\rangle_{\ell,\alpha}=\frac{ie}{2\hbar}\langle\nabla_{\mathbf{k}}u_{\ell\alpha}(\mathbf{k})\Big|(\epsilon_\ell(\mathbf{k})-\hat{H})\times\Big|\nabla_{\mathbf{k}}u_{\ell\alpha}(\mathbf{k})\rangle. \tag{C2}$$

Noting that for the two-band, particle-hole symmetric system $\epsilon_{\ell=+}(\mathbf{k})=-\epsilon_{\ell=-}(\mathbf{k})$ we have

$$\epsilon_\ell(\mathbf{k})-\hat{H}_\alpha=2\epsilon_\ell(\mathbf{k})|u_{n\neq\ell,\alpha}(\mathbf{k})\rangle\langle u_{n\neq\ell,\alpha}(\mathbf{k})| \tag{C3}$$

Inserting into the Eq. (C2) we obtain

$$\langle\hat{\mathbf{M}}\rangle_{\ell,\alpha}=\frac{ie\epsilon_\ell}{\hbar}\Big[\Big\langle\frac{\partial u_{\ell,\alpha}}{\partial k_x}\Big|\frac{\partial u_{\ell,\alpha}}{\partial k_y}\Big\rangle-\Big\langle\frac{\partial u_{\ell,\alpha}}{\partial k_y}\Big|\frac{\partial u_{\ell,\alpha}}{\partial k_x}\Big\rangle\Big] \tag{C4}$$

where we have applied the resolution of the identity. Recalling that the Berry curvature is simply $\mathbf{\Omega}_{\ell\alpha}(\mathbf{k})=i\langle\nabla_{\mathbf{k}}u_{\ell\alpha}(\mathbf{k})\,|\times|\,\nabla_{\mathbf{k}}u_{\ell\alpha}(\mathbf{k})\rangle$, we obtain Eq. (C1).

Appendix D: Alternative derivation of inhomogeneous current density: velocity matrix element

In this section, we discuss an alternative algebraic derivation of the inhomogeneous current density by expanding the velocity matrix element at finite $\mathbf{q}$. For brevity, we will suppress the flavor index α leaving only the band index l without loss of any generality. While less compact than the above discussion (using the magnetic moment operator), this alternative approach explicitly shows how the accumulation of geometric phases at finite $\mathbf{q}$ leads to the anomalous transverse diffusion.

We proceed by considering the current dynamics in Bloch bands with a spatially varying out-of-equilibrium carrier density in the absence of an applied magnetic field. The current density $\mathbf{j}_l(\mathbf{r})=e\sum_{\mathbf{q}}\mathbf{v}_{\mathbf{q}}^{(l)}e^{i\mathbf{q}\cdot\mathbf{r}}$, can be expressed in terms of its Fourier harmonics as

$$\mathbf{v}_{\mathbf{q}}^{(l)}=\sum_{\mathbf{k}}c^\dagger_{\mathbf{k}_-,l}\langle l,\mathbf{k}_-|\hat{\mathbf{v}}|l,\mathbf{k}_+\rangle c_{\mathbf{k}_+,l},\quad \hbar\hat{\mathbf{v}}=\frac{\partial\hat{H}}{\partial\mathbf{k}}, \tag{D1}$$

where $\hat{\mathbf{v}}$ is the velocity operator, $\hat{H}$ is the hamiltonian, $\mathbf{k}_\pm=\mathbf{k}+\mathbf{q}/2$, $c^\dagger_{\mathbf{k},l}$ is a creation operator for quasiparticles in band l with corresponding (Bloch) wavefunction $\langle\mathbf{r}|c^\dagger_{\mathbf{k},l}|0\rangle=\langle\mathbf{r}|l,\mathbf{k}\rangle e^{i\mathbf{k}\cdot\mathbf{r}}$. The crystal wavefunctions $\langle\mathbf{r}|n,\mathbf{k}\rangle=u_{l,\mathbf{k}}(\mathbf{r})$ are periodic over the unit cell.

As we now demonstrate, the phases accumulated by quasiparticles in the bands can play a crucial role in their transport, producing anomalous current flow when the carrier density is inhomogeneous. To illustrate this, we first note that the wavefunction $\langle\mathbf{r}|l,\mathbf{k}+\mathbf{q}\rangle$ can be expanded, to leading order in $\mathbf{q}$, as

$$\langle\mathbf{r}|l,\mathbf{k}\rangle+\Big(\langle\mathbf{r}|\frac{\partial u_{l,\mathbf{k}}}{\partial\mathbf{k}_i}\rangle-i\mathcal{A}_{l,i}(\mathbf{k})\langle\mathbf{r}|u_{l,\mathbf{k}}\rangle\Big)\mathbf{q}_i+\cdots, \tag{D2}$$

where we have expressed the expansion in component form, and $\mathcal{A}_{l,i}(\mathbf{k})=\boldsymbol{\mathcal{A}}_l(\mathbf{k})\cdot\hat{\mathbf{x}}_i$ is the i^{th} component of the Berry connection $\boldsymbol{\mathcal{A}}_l(\mathbf{k})=i\langle u_{l,\mathbf{k}}|\partial_{\mathbf{k}}|u_{l,\mathbf{k}}\rangle$ (i.e. $\boldsymbol{\mathcal{A}}_l$ in the $\hat{\mathbf{x}}_i$ direction). Notice that the Taylor expansion in $\mathbf{k}$ is done using the covariant derivative, $\boldsymbol{\nabla}_{\mathbf{k}}=\partial_{\mathbf{k}}-i\boldsymbol{\mathcal{A}}_l(\mathbf{k})$: this is needed to ensure that the calculated current is physical, i.e., invariant under a "gauge transformation" of the crystal wave function, $u_{l,\mathbf{k}}(\mathbf{r})\to e^{-i\chi(\mathbf{k})}u_{l,\mathbf{k}}(\mathbf{r})$.

Applying the expansion of the wavefunction at small $\mathbf{q}$ described in Eq. (D2) to the velocity matrix element, we obtain

$$\langle l,\mathbf{k}_-|\hat{\mathbf{v}}_i|l,\mathbf{k}_+\rangle=\langle l,\mathbf{k}|\hat{\mathbf{v}}_i|l,\mathbf{k}\rangle+[\boldsymbol{\mathcal{C}}^{(l)}_{ij}(\mathbf{k})](i\mathbf{q}_j)+\mathcal{O}(q^2), \tag{D3}$$

where $\hbar\langle l,\mathbf{k}|\hat{\mathbf{v}}_i|l,\mathbf{k}\rangle=\frac{\partial\epsilon_l(\mathbf{k})}{\partial\mathbf{k}_i}$ is the group velocity, and

$$\begin{aligned}[\boldsymbol{\mathcal{C}}^{(l)}_{ij}(\mathbf{k})](i\mathbf{q}_j)&=\left[\Big\langle\frac{\partial u_{l,\mathbf{k}}}{\partial\mathbf{k}_j}\Big|\hat{\mathbf{v}}_i\Big|u_{l,\mathbf{k}}\Big\rangle-\Big\langle u_{l,\mathbf{k}}\Big|\hat{\mathbf{v}}_i\Big|\frac{\partial u_{l,\mathbf{k}}}{\partial\mathbf{k}_j}\Big\rangle\right]\frac{\mathbf{q}_j}{2}-2i\langle u_{l,\mathbf{k}}|\hat{\mathbf{v}}_i|u_{l,\mathbf{k}}\rangle\mathcal{A}_j\frac{\mathbf{q}_j}{2}\\&=\sum_m\left[\Big\langle\frac{\partial u_{l,\mathbf{k}}}{\partial\mathbf{k}_j}\Big|u_{m,\mathbf{k}}\Big\rangle\langle u_{m,\mathbf{k}}|\hat{\mathbf{v}}_i\Big|u_{l,\mathbf{k}}\Big\rangle-\Big\langle u_{l,\mathbf{k}}\Big|\hat{\mathbf{v}}_i\Big|u_{m,\mathbf{k}}\Big\rangle\langle u_{m,\mathbf{k}}|\frac{\partial u_{l,\mathbf{k}}}{\partial\mathbf{k}_j}\Big\rangle\right]\frac{\mathbf{q}_j}{2}-2i\langle u_{l,\mathbf{k}}|\hat{\mathbf{v}}_i|u_{l,\mathbf{k}}\rangle\mathcal{A}_j\frac{\mathbf{q}_j}{2}.\end{aligned} \tag{D4}$$

In the last line we have inserted the resolution of the identity $\sum_m|u_{m,\mathbf{k}}\rangle\langle u_{m,\mathbf{k}}|=1$ into the terms of the square parentheses.

In order to proceed, we note that when $m=l$, the square parentheses cancel with the last term since $\langle u_{l,\mathbf{k}}|\frac{\partial u_{l,\mathbf{k}}}{\partial\mathbf{k}_j}\rangle=-i\mathcal{A}_j$. As a result, only terms with $m\neq l$ remain in Eq. (D4). Using the identity for the interband matrix element

$$\hbar\langle u_{l,\mathbf{k}}|\hat{\mathbf{v}}_i|u_{m,\mathbf{k}}\rangle=\langle u_{l,\mathbf{k}}|\frac{\partial u_{m,\mathbf{k}}}{\partial k_i}\rangle[\epsilon_l(\mathbf{k})-\epsilon_m(\mathbf{k})],\quad l\neq m, \tag{D5}$$

where $\epsilon_l(\mathbf{k})$ is the quasiparticle energy in band l, yields

$$\boldsymbol{\mathcal{C}}^{(l)}_{ij}=-\frac{i}{2\hbar}\sum_{m\neq l}\langle\frac{\partial u_{l,\mathbf{k}}}{\partial k_i}|u_{m,\mathbf{k}}\rangle[\epsilon_l(\mathbf{k})-\epsilon_m(\mathbf{k})]\langle u_{m,\mathbf{k}}|\frac{\partial u_{l,\mathbf{k}}}{\partial k_j}\rangle-c.c. \tag{D6}$$

Comparing this with the well known expression for the magnetic moment[19,20]

$$\langle\hat{\mathbf{M}}\rangle = \frac{ie}{2\hbar}\langle\nabla_{\mathbf{k}}u_{l\alpha}(\mathbf{k})\left|(\epsilon_{l\alpha}(\mathbf{k})-\hat{H})\times\right|\nabla_{\mathbf{k}}u_{l\alpha}(\mathbf{k})\rangle \quad \text{(D7)}$$

yields Eq. (3) of the main text.

Appendix E: Estimate of characteristic SEC resistivity

In the following we give a simple estimate of the characteristic SEC resistivity. Recalling Eq. (12) of the main text, we have the resistivity of the SEC channel

$$\rho_{1\mathrm{d}}(T) = \frac{\rho_0}{\tilde{\beta}^{1/2}\mathcal{F}(\tilde{\beta})}, \quad \rho_0 = \frac{2\Delta^{3/2}(\eta/e)^{1/2}}{\hbar v^2\tau_v^{1/2}|\sigma_H^v|}, \qquad \text{(E1)}$$

where ρ_0 is the characteristic 1D resistivity and can be estimated as

$$\rho_0 = 0.48\frac{(\Delta[\mathrm{meV}]/10)^{3/2}(\eta[\mathrm{m}^2/\mathrm{Vs}])^{1/2}}{(\tau_v[\mathrm{ps}]/10)^{1/2}}\left[\frac{h}{e^2}\mu\mathrm{m}^{-1}\right], \qquad \text{(E2)}$$

where we have used $v = 10^6\,\mathrm{m/s}$, and taken $|\sigma_H^v| = 2e^2/h$.

We note that for narrow-gapped Dirac materials $\Delta \sim 10\,\mathrm{meV}$, ρ_0 can be as small as fractions of the quantum of resistance h/e^2. As a result, at low temperatures, $\rho_{1\mathrm{d}}(T)$ in Eq. E1 yielding low-dissipation squeezed edge channels. When the values for ρ_0 in Eq. E1 for such narrow-gapped Dirac materials is substituted into Eq. 10, we find the low-dissipation $\rho_{1d}L$ can become far smaller than R_{contact}. As a result, R_{SEC} (red line in Fig. 2b) becomes dominated by R_{contact} and tends to R_{contact} (dashed line in Fig. 2b) value at low-temperature.

As discussed in the main text, this behavior was recently seen in gapped graphene-type structures Ref.[18] where a saturation of device resistance (up to a few resistance quanta) was measured in Hall bars even at low temperatures ($\sim 10\,\mathrm{K}$) (where SEC is operative); while Corbino geometry measurements (where edge contributions are eliminated) of the same samples showed fully activated behavior.

In contrast, for large gapped Dirac materials $\Delta \sim 1\,\mathrm{eV}$, ρ_0 can be many times larger; for e.g., taking $\Delta = 1\mathrm{eV}$ and $\eta = 1\mathrm{m}^2/\mathrm{Vs}$ and $\tau_v = 1\mathrm{ps}$ we obtain a very resistive channel $\rho_0 \approx 40\,\mathrm{M}\Omega\mu\mathrm{m}^{-1}$. These values are so large as to be comparable with the bulk resistance making SEC ineffective current shunts to bulk charge current conduction.

As a result, we conclude that narrow-gapped Dirac materials (e.g., G/hBN or gapped bilayer graphene) at low temperature are ideal platforms to observe low-dissipation squeezed edge currents (as seen in Fig. 2 of the main text; compare also with Hall bar device resistances observed in Ref.[18]).